Advances in Differential Equations and Control Processes 2025, 32(1), 2759.
https://doi.org/10.59400/adecp2759

Article

Herd immunity in a coronavirus disease 2019 epidemic model with consideration of vaccination and quarantine interventions

Moh Hasan*, Faizal Rifky Fahreza

Department of Mathematics, University of Jember, Jember 68121, Indonesia
*** Corresponding author:** Moh Hasan, hasan.fmipa@unej.ac.id

CITATION

Hasan M, Fahreza FR. Herd immunity in a coronavirus disease 2019 epidemic model with consideration of vaccination and quarantine interventions. Advances in Differential Equations and Control Processes. 2025; 32(1): 2759. https://doi.org/10.59400/adecp2759

ARTICLE INFO

Received: 10 February 2025
Accepted: 12 March 2025
Available online: 21 March 2025

Abstract: During the pandemic of COVID-19, people had reduced contact among each other. As a result of this behavior, several factors, such as economic conditions and the teaching and learning process, have been affected. Hence, it is important to identify whether the impact of COVID-19 is no longer as severe as when it was first observed. The study aimed to analyze herd immunity against COVID-19 in Indonesia according to the bifurcations and simulations of mathematical models of COVID-19 transmission. Based on the bifurcation of the disease system, whether the current pandemic was controlled with standard interventions was evaluated. The system behavior can be compared with herd immunity that should be achieved in a specific population. Thus, whether a system has resulted in the achievement of herd immunity can be evaluated. The behavior of this system can provide information on the achievement of group immunity during disease outbreaks.

Keywords: herd immunity threshold; infection rate, bifurcation diagram; basic reproduction number

1. Introduction

The mathematical compartment models of infectious disease transmission can provide an overview of disease dynamics [1]. The compartment model is built based on assumptions regarding the natural behavior of disease, which can simply be used to predict the peak point of disease transmission in a specific population [2–4]. The assumptions used in building disease distribution models are not limited to the natural behavior of diseases. Moreover, models can also be built by considering interventions or other factors such as migration [5], social restrictions or confinement [6], and implementation of vaccination and quarantine [7,8]. Using the mathematical models of infectious disease, we can exert efforts to control disease transmission [9,10], determine the efficacy of interventions [8,11], and view disease conditions based on models such as herd immunity conditions [12,13], where the condition of herd immunity in an outbreak can simply be demonstrated by simulating a model [12].

The compartment model of infectious disease transmission, which is built by several differential equations, is a continuous dynamical system. In a dynamical system, we can see how the system behaves. One of them is a change in system behavior if there is an alteration in the parameters of the system. Bifurcation is the instrument used to identify this change [14,15]. In a compartmental model of disease transmission, a bifurcation can appear as two types, namely, backward bifurcation and forward bifurcation, both of which can be explained graphically via a bifurcation diagram [1,16,17]. Via an analysis of this bifurcation, we can have an idea on whether the disease can disappear if standard interventions are carried out or how difficult it is

to control the disease during epidemic [18,19]. Further, bifurcation can be used to identify the efficacy of a parameter in making the disease system more controllable [20]. That is, it can assess vaccine efficacy and the appropriate vaccine timing, which can make the system more controlled [21].

Currently, we are experiencing the coronavirus disease 2019 (COVID-19) outbreak. COVID-19 has a unique transmission behavior. Hence, the disease outbreak, which is still experienced in Indonesia, has been interesting, and it can be assessed more deeply in terms of the mathematical models of disease transmission. Data have shown an increase in the number of COVID-19 cases in Indonesia during specific periods even after the implementation of vaccination. That is, the incidence of COVID-19 was high after school or year-end holidays [22]. In addition, the interventions carried out by the government, such as the implementation of health protocols in public spaces, vaccinations, and social restrictions, had an influence on the transmission process of COVID-19 in society [23,24]. Hence, the current status of the COVID-19 outbreak is interesting to assess when viewed from the epidemic model. Moreover, the interventions that can suppress the transmission of COVID-19 in society should be evaluated.

The use of mathematical modeling, particularly through bifurcation analysis, offers significant advantages in understanding the dynamics of COVID-19 spread. This approach facilitates the simulation of various scenarios related to virus transmission, enabling the prediction of infection wave peaks and troughs while identifying key factors that influence transmission. By employing bifurcation analysis, critical points can be pinpointed where minor changes in parameters may lead to substantial shifts in spread dynamics, including the attainment of herd immunity conditions. Consequently, mathematical modeling serves as a valuable tool in designing effective intervention strategies, appropriately allocating health resources, and ultimately controlling the pandemic.

This study aims to evaluate the achievement of herd immunity against COVID-19 in Indonesia through bifurcation analysis and the simulation of a mathematical model for the virus. Specifically, the objectives of this research are: (1) To determine whether Indonesia has attained herd immunity based on model analysis; (2) to estimate parameters, identify the type of basic reproduction number, and conduct a sensitivity analysis of parameters to reinforce the simulation results; (3) to predict future system behavior using bifurcation and compartment model simulations; and (4) to examine the unique distribution patterns of COVID-19 data in Indonesia. Ultimately, this study aims to provide a comprehensive understanding of the dynamics of COVID-19 spread and the status of herd immunity in Indonesia through a mathematical modeling approach.

To evaluate herd immunity against COVID-19 in Indonesia, we utilized bifurcations and simulations based on a mathematical model. The model will be analyzed in the final phase of data collection in this study. Other supporting processes such as parameter estimation, identification of the type of the basic reproduction number of the system, and sensitivity analysis of the parameters in the system will also be performed to support the results of the system simulation. Using data obtained at the final phase as the starting point for the simulation, the behavior of the system in the future when viewed from the bifurcations produced by the system and the

simulation of each compartment in the disease transmission system will be examined. Finally, the unique distribution pattern of data on COVID-19 in Indonesia was investigated.

2. Methods

A COVID-19 transmission model was examined with consideration of vaccination and quarantine interventions [25]. Since it was more pertinent to current intervention efforts against COVID-19, this model would have been updated by adding a booster vaccine compartment. The model was first fit to data that have been divided into several phases of the disease distribution period to obtain estimated results from the parameters of vaccination rate for doses 1, 2, and booster (φ_1, φ_2, and φ_3), recovery rate (γ), rate of movement from compartments $I(t)$ to $Q(t)$ (τ_1), and the COVID-19 mortality rate (ζ). Next, the equation of the basic reproduction number ($\mathcal{R}_0$) of the model was examined using the next-generation matrix. Then, by taking the force of infection parameter $\left(\beta^* = \frac{\lambda I^* + \lambda q Q^*}{N}\right)$, bifurcations in the system regarding the basic reproduction number ($\mathcal{R}_0$) were assessed. Next, a sensitivity analysis was performed to determine parameters with changes that can significantly affect the basic reproduction number. Finally, a simulation was run on the model to determine its behavior up to day 1800 (t). The numerical simulations are applied in PYTHON using the fourth-order Runge-Kutta method.

3. Results and discussion

Initially, the model presented in [25] is adjusted to include a booster vaccination compartment, resulting in the updated model depicted in Equation (1), with the used variables in Equation (1) described in **Table 1**. This modification aims to reflect the impact of booster vaccinations on the dynamics of the epidemiological model.

$$
\begin{aligned}
\frac{dS}{dt} &= \Lambda - \frac{\lambda SI}{N} - \frac{\lambda qSQ}{N} - \varphi_1 S + \rho R - \mu S,\\
\frac{dV_1}{dt} &= \varphi_1 S - \frac{\lambda pV_1 I}{N} - \frac{\lambda pqV_1 Q}{N} - \varphi_2 V_1 - \mu V_1,\\
\frac{dV_2}{dt} &= \varphi_2 V_1 - \frac{\lambda rV_2 I}{N} - \frac{\lambda rqV_2 Q}{N} - \varphi_3 V_2 - \mu V_2,\\
\frac{dV_3}{dt} &= \varphi_3 V_2 - \frac{\lambda sV_3 I}{N} - \frac{\lambda sqV_3 Q}{N} - \mu V_3,\\
\frac{dI}{dt} &= \frac{\lambda SI}{N} + \frac{\lambda pV_1 I}{N} + \frac{\lambda rV_2 I}{N} + \frac{\lambda sV_3 I}{N} + \frac{\lambda qSQ}{N} + \frac{\lambda pqV_1 Q}{N} + \frac{\lambda rqV_2 Q}{N} + \frac{\lambda sqV_3 Q}{N} - \tau_1 I + \tau_2 Q - \gamma I - \zeta I - \mu I,\\
\frac{dQ}{dt} &= \tau_1 I - \tau_2 Q - \gamma Q - \zeta dQ - \mu Q,\\
\frac{dR}{dt} &= \gamma I + \gamma Q - \rho R - \mu R,\\
\frac{dD}{dt} &= \zeta I + \zeta dQ.
\end{aligned}
\tag{1}
$$

Table 1. Variables in the model.

Variables	Description	Variables	Description
S	Susceptible compartment (individuals susceptible to COVID-19).	q	Reduced rate of infection due to quarantine.
V_1	Compartment of individuals who have received one dose of the vaccine.	p	Reduced rate of infection due to the first vaccine dose.
V_2	Compartment of individuals who have received two doses of the vaccine.	r	Reduced rate of infection due to the second vaccine dose.
V_3	Compartment of individuals who have received a vaccine booster dose.	s	Reduced rate of infection due to the vaccine booster dose.
I	Compartment of individuals exposed to COVID-19.	τ_1	The rate of movement from $I(t)$ to $Q(t)$.
Q	Compartment of individuals who were quarantined.	τ_2	The rate of movement from $Q(t)$ to $I(t)$.
R	Compartment of individuals who have recovered from COVID-19.	γ	Recovery rate.
D	Compartment of individuals who have died from COVID-19.	ζ	COVID-19 mortality rate.
λ	Infection rate.	ρ	Reinfection rate.
φ_1	First-dose vaccination rate.	d	Reduced mortality rate due to vaccination.
φ_2	Second-dose vaccination rate.	μ	Normal mortality rate.
φ_3	Booster-dose vaccination rate.	Λ	Normal birth rate.

The λ parameter is pivotal as it represents the infection rate in disease transmission dynamics. Specifically, λ indicates the speed at which a disease can be transmitted from an infected individual to a susceptible one. A high λ value suggests a greater potential for transmission, which can quickly accelerate the spread of the disease within a population. Conversely, a low λ value signifies a slower transmission rate, thereby allowing more time for interventions like quarantine and vaccination to mitigate spread. Understanding and managing λ is therefore critical in forecasting and addressing the impact of disease outbreaks. Given the significant influence of λ on disease dynamics, the next simulation will explore variations in its value. This exploration aims to thoroughly examine how alterations in the infection rate can affect the overall behavior of the system, ultimately providing deeper insights into transmission patterns and informing the development of more effective control strategies.

The data used in this study starts from the implementation of vaccination interventions in Indonesia, which are divided into six phases. The first phase was from 25 May 2021 to 8 August 2021. In this phase, the most significant increase in the number of cases was observed, and this period occurred after the holidays. Further, vaccination was implemented only in a small population of individuals in Indonesia. The second phase was from 9 August 2021 to 20 January 2022. The number of cases in this phase began to decrease until it entered the next phase. The third phase was from 21 January 2022 to 22 March 2022. The events in this phase were similar to those in the first phase. That is, there was a fairly high increase in cases. Moreover, this phase occurred after the holidays at the start of 2022. Booster dose vaccinations are also started at this phase. The fourth phase was from 23 March 2022 to 19 July 2022. In this phase, the number of cases began to decrease again until it entered the fifth phase. The fifth phase was from 20 July 2022 to 14 November 2022. In this phase, there was a fairly high increase in the number of cases. However, it was not as high as

the previous phase. Notably, this phase occurred after the school holidays, which have a high population mobilization. The final phase was from 15 November 2022 to 21 August 2023. During this phase, the number of cases began to decrease again. After dividing the data into several phases according to data behavior, parameter estimation and numerical simulations were then performed to identify the behavior of the system using data on the distribution of COVID-19 in Indonesia.

3.1. Parameter estimation

The values of the parameters in the model could be estimated using the Levenberg-Marquardt method. The estimation process was performed by fitting the model to COVID-19 data in Indonesia. The model was fitted to the six time periods described previously. Next, the parameter values were estimated as λ, φ_1, φ_2, φ_3, τ_1, γ, and ζ. Then, the other parameter values were assumed. **Table 2** shows the assumed parameter values.

Table 2. Assumed parameter values.

Parameters	Values	Description	Parameters	Values	Description
τ_2	0.002857	The rate of movement from $Q(t)$ to $I(t)$ [25].	q	0.05	Reduced rate of infection due to quarantine [25].
ρ	0.0065	Reinfection rate [26].	d	0.02	Reduced mortality rate due to vaccine [25].
p	0.590071	Reduced rate of infection due to one dose of the vaccine [25].	Λ	μN	Normal birth rate.
r	0.180143	Reduced rate of infection due to two-dose vaccine [25].	μ	0.1/100	Normal mortality rate.
s	0.05	Reduced rate of infection due to the vaccine booster dose.			

The parameter estimation process was carried out at each phase. The parameter estimates for each phase used different compartment initial values according to data on the distribution of COVID-19 at the beginning of each phase. Then, by estimating in the range $[0,1]$ with an initial guess of the estimated parameter of 1, the parameter estimation results were obtained, as presented in **Table 3**.

Table 3. Parameter estimation results.

Parameters	Phase 1	Phase 2	Phase 3	Phase 4	Phase 5	Phase 6
φ_1	2.6573×10^{-5}	2.2537×10^{-5}	1.1967×10^{-7}	2.0318×10^{-9}	2.1838×10^{-7}	4.0022×10^{-8}
φ_2	0.00404883	3.2261×10^{-8}	0.02138271	0.01665606	6.3478×10^{-4}	0.20056574
φ_3	9.2184×10^{-4}	0.01048115	0.00980319	0.04317824	2.4659×10^{-8}	1.2903×10^{-4}
λ	0.15726904	0.01516746	0.21959746	0.40082814	0.01847884	0.01675573
τ_1	0.21450170	0.23739794	0.10843339	0.40929794	0.01773789	0.03731990
γ	0.00325502	4.3557×10^{-4}	0.03614694	0.03712054	0.01526998	0.00596946
ζ	9.3787×10^{-4}	0.01578178	0.04053776	0.17200603	7.8497×10^{-5}	0.01750052

3.2. Basic reproduction number ($\mathcal{R}_0$)

The basic reproduction number (secondary infection) of the model was obtained using the next-generation matrix. Before finding the equation that defines $\mathcal{R}_0$, we first identified the disease-free equilibrium point. In disease-free conditions, disease transmission in the population was considered non-existent. Hence, the value for $I = Q = R = D = 0$ was obtained. Next, by applying $S'(t) = V_1'(t) = V_2'(t) = V_3'(t) = I'(t) = Q'(t) = R'(t) = D'(t) = 0$, we obtained:

$$E^0 = (S^0, V_1^0, V_2^0, V_3^0, I^0, Q^0, R^0, D^0) = \left(\frac{\Lambda}{k_1}, \frac{\varphi_1\Lambda}{k_1k_2}, \frac{\varphi_2\varphi_1\Lambda}{k_1k_2k_3}, \frac{\varphi_3\varphi_2\varphi_1\Lambda}{k_1k_2k_3\mu}, 0,0,0,0\right),$$

with $k_1 = \varphi_1 + \mu$, $k_2 = \varphi_2 + \mu$, $k_3 = \varphi_3 + \mu$.

When the disease-free equilibrium (DFE) state was observed, it was evident that the first vaccination dosage (φ_1) would cause the susceptible compartment, represented by $S(t)$, to continuously decrease. Similarly, it was observed that the transition rates between the first and second vaccination dose compartments caused them to decrease. On the other hand, the booster vaccination dose compartment was expected to grow as a result of the new people moving into that compartment from the previous one.

Then, by using the next generation matrix $\left(\mathbf{K} = \mathbf{FV^{-1}}\right)$ in the infected compartment in model (1), namely, compartments $I(t)$ and $Q(t)$, the matrix $\boldsymbol{\mathcal{F}}$, which is the rate of new infections, and $\boldsymbol{\mathcal{V}}$, which is the rate of movement of infected individuals, were obtained as follows:

$$\boldsymbol{\mathcal{F}} = \begin{bmatrix} \dfrac{\lambda SI + \lambda qSQ + \lambda pV_1I + \lambda pqV_1Q + \lambda rV_2I + \lambda rqV_2Q + \lambda sV_3I + \lambda sqV_3Q}{N} \\ 0 \end{bmatrix},$$

$$\boldsymbol{\mathcal{V}} = \begin{bmatrix} k_4I - \tau_2Q \\ k_5Q - \tau_1I \end{bmatrix},$$

with $k_4 = \tau_1 + \gamma + \zeta + \mu, k_5 = \tau_2 + \gamma + \zeta d + \mu$.

Then, the matrices **F** and **V** can be obtained as follows:

$$\mathbf{F} = \begin{bmatrix} \dfrac{\partial \mathcal{F}_1}{\partial I} & \dfrac{\partial \mathcal{F}_1}{\partial Q} \\ \dfrac{\partial \mathcal{F}_2}{\partial I} & \dfrac{\partial \mathcal{F}_2}{\partial Q} \end{bmatrix} = \begin{bmatrix} \dfrac{\lambda(S + pV_1 + rV_2 + sV_3)}{N} & \dfrac{\lambda q(S + pV_1 + rV_2 + sV_3)}{N} \\ 0 & 0 \end{bmatrix},$$

$$\mathbf{V} = \begin{bmatrix} \dfrac{\partial \mathcal{V}_1}{\partial I} & \dfrac{\partial \mathcal{V}_1}{\partial Q} \\ \dfrac{\partial \mathcal{V}_2}{\partial I} & \dfrac{\partial \mathcal{V}_2}{\partial Q} \end{bmatrix} = \begin{bmatrix} k_4 & -\tau_2 \\ -\tau_1 & k_5 \end{bmatrix}.$$

The next generation matrix is obtained as follows:

$$\mathbf{K} = \mathbf{FV^{-1}},$$
$$= \begin{bmatrix} \dfrac{\lambda(V_1p + V_2r + V_3s + S)(q\tau_1 + k_5)}{N(k_4k_5 - \tau_1\tau_2)} & \dfrac{\lambda(V_1p + V_2r + V_3s + S)(qk_4 + \tau_2)}{N(k_4k_5 - \tau_1\tau_2)} \\ 0 & 0 \end{bmatrix}.$$

Furthermore, the $\mathcal{R}_0$ equation from the model is the spectral radius of the **K** matrix. Hence, the $\mathcal{R}_0$ equation is obtained as follows:

$$\mathcal{R}_0 = \frac{\lambda(V_1 p + V_2 r + V_3 s + S)(q\tau_1 + k_5)}{N(k_4 k_5 - \tau_1 \tau_2)} \tag{2}$$

Next, by substituting E^0 into Equation (2), we obtain the basic reproduction number equation as follows:

$$\mathcal{R}_0 = \frac{(k_5 + q\tau_1)(\mu(p\varphi_1 + k_2)k_3 + \varphi_2(\mu r + s\varphi_3)\varphi_1)\lambda}{k_1 k_2 k_3\big(k_5(\gamma + \mu + \zeta) + \tau_1(d\zeta + \gamma + \mu)\big)} \tag{3}$$

According to the equation $\mathcal{R}_0$, the infection rate (λ), the reduction in infection rate due to quarantine (q), and the reduction in infection rate due to the first dose of vaccination to the booster (p, r, s) are important factors in determining the value of $\mathcal{R}_0$ in the system. As the rate of disease transmission (λ) increases, correspondingly increases the value of $\mathcal{R}_0$. In contrast, the reduction in infection rate due to vaccination (p, r, s), which is related to vaccine efficacy, tends to decrease $\mathcal{R}_0$ towards zero as efficacy approaches 100%. This demonstrates that higher vaccine efficacy leads to lower $\mathcal{R}_0$ values. Similarly, the parameter representing the reduction in disease transmission due to quarantine (q) shows that as compliance with the quarantine protocol increases, this value approaches zero, resulting in a decrease in the system's $\mathcal{R}_0$ value. After obtaining Equation (3), the corresponding $\mathcal{R}_0$ values for Model (1) are depicted in **Table 4**.

Table 4. Basic reproduction number in each phase.

	Phase 1	**Phase 2**	**Phase 3**	**Phase 4**	**Phase 5**	**Phase 6**
$\mathcal{R}_0$	2.8842	0.5003	1.3933	0.9872	0.615	0.3864

It can be seen from **Table 4**, phase 1 has the highest $\mathcal{R}_0$ value. This is consistent with the fact that vaccination attempts are still in their early stages and that this phase occurs after the holiday period, increasing the risk of COVID-19 transmission. In contrast, phase 2 shows a $\mathcal{R}_0$ value below 1, indicating a decrease in transmission rates. This matches the giving of up to two vaccine doses on a larger scale. However, in phase 3, the value of $\mathcal{R}_0$ increased and exceeded 1, but the secondary infection rate did not reach the same value as in phase 1. This increase in cases could be due to the post-year-end period, which is typically characterized by an increase in population movement, making individual interactions more frequent. During this phase, booster vaccine administration has also begun, and the impact on secondary infection rates will be observed later. Next, phases 4 to 6 are characterized by a consistent decrease in the value of $\mathcal{R}_0$. Notably, even after the school holidays in phase 5, the secondary infection rate remained below 1 and did not exceed the value in the previous phase. Overall, the data shows that vaccine implementation, particularly booster shots, has been effective in dealing with secondary infections in the system. Additionally, the continuous decrease in the value of $\mathcal{R}_0$ from phases 4 to 6 may also be an indication that the system is heading towards a herd immunity state, a hypothesis that will be further explored with additional simulation tools.

3.3. Bifurcation analysis

Bifurcation will be sought by finding the endemic equilibrium of model (1). Let $E^* = (S^*, V_1^*, V_2^*, V_3^*, I^*, Q^*, R^*, D^*)$ be the endemic equilibrium of model (1). Then, let the force of infection.

$$\beta^* = \frac{\lambda I^* + \lambda q Q^*}{N} \tag{4}$$

Next, by making model (1) equal to 0, it will be obtained as follows:

$$\begin{aligned}
S^* = {} & [(-k_4k_5 + \tau_1\tau_2)(\beta^* r + k_3)(\beta^* s + \mu)(\beta^* p + k_2)k_6\Lambda] \\
& / \Big[\big((-k_4k_5 + \tau_1\tau_2)k_6 + \rho\gamma(k_5 + \tau_1)\big)rsp\beta^{*4} \\
& + \Big(\big(\big((k_1 s + \mu)r + sk_3\big)p + rsk_2\big)(-k_4k_5 + \tau_1\tau_2)k_6 + \big(\big((s\varphi_1 + \mu)r + sk_3\big)p + rsk_2\big)\rho(k_5 + \tau_1)\gamma\Big)\beta^{*3} \\
& + \Big(\big(\big(k_1 r\mu + k_3(k_1 s + \mu)\big)p + \big((k_1 s + \mu)r + sk_3\big)k_2\big)(-k_4k_5 + \tau_1\tau_2)k_6 \\
& + \rho(k_5 + \tau_1)\gamma\big(\big(\mu\varphi_1 r + k_3(s\varphi_1 + \mu)\big)p + (s\varphi_1\varphi_2 + k_2\mu)r + sk_2k_3\big)\Big)\beta^{*2} \\
& + \Big(\big(p\mu k_1k_3 + \big(k_1 r\mu + k_3(k_1 s + \mu)\big)k_2\big)(-k_4k_5 + \tau_1\tau_2)k_6 \\
& + \rho\gamma(k_5 + \tau_1)(k_3\mu p\varphi_1 + \mu r\varphi_1\varphi_2 + s\varphi_1\varphi_2\varphi_3 + k_2k_3\mu)\Big)\beta^* + \mu k_1k_2k_3k_6(-k_4k_5 + \tau_1\tau_2)\Big] \\
V_1^* = {} & [\varphi_1\Lambda k_6(k_4k_5 - \tau_1\tau_2)(\beta^* r + k_3)(\beta^* s + \mu)] \\
& / \Big[-\Big(\big(\rho\gamma\varphi_1 + \tau_2k_6k_1 + \beta^*(\rho\gamma + k_6\tau_2)\big)\tau_1 + \big(\rho\gamma\varphi_1 - k_4k_6k_1 + \beta^*(\rho\gamma - k_4k_6)\big)k_5\Big)\beta^*(\beta^* s + \mu)(\beta^* r + k_3)p \\
& - (\beta^* s + \mu)\Big(\big(\tau_2k_6k_1 + \beta^*(\rho\gamma + k_6\tau_2)\big)\tau_1 + \big(-k_4k_6k_1 + \beta^*(\rho\gamma - k_4k_6)\big)k_5\Big)(\beta^* r + k_3)k_2 \\
& - \big(\mu r + s(\beta^* r + \varphi_3)\big)\varphi_2\rho\beta^*(k_5 + \tau_1)\gamma\varphi_1\Big] \\
V_2^* = {} & [(k_4k_5 - \tau_1\tau_2)(\beta^* s + \mu)k_6\Lambda\varphi_1\varphi_2] \\
& / \Big[-(\beta^* + k_1)(\beta^* r + k_3)(-k_4k_5 + \tau_1\tau_2)(\beta^* s + \mu)(\beta^* p + k_2)k_6 \\
& - \Big(\beta^{*3}prs + (prs\varphi_1 + (k_2 r + k_3 p)s + \mu pr)\beta^{*2} + \big(\big(rs\varphi_2 + p(sk_3 + \mu r)\big)\varphi_1 + sk_2k_3 + (k_2 r + k_3 p)\mu\Big)\beta^* \\
& + \big((\mu r + s\varphi_3)\varphi_2 + k_3 p\mu\big)\varphi_1 + k_2k_3\mu\Big)\rho\beta^*(k_5 + \tau_1)\gamma\Big] \\
V_3^* = {} & [\varphi_3\varphi_2\varphi_1\Lambda k_6(-k_4k_5 + \tau_1\tau_2)] \\
& / \Big[\big((-k_4k_5 + \tau_1\tau_2)k_6 + \rho\gamma(k_5 + \tau_1)\big)rsp\beta^4 \\
& + \Big(\big(\big((k_1 s + \mu)r + sk_3\big)p + rsk_2\big)(-k_4k_5 + \tau_1\tau_2)k_6 + \big(\big((s\varphi_1 + \mu)r + sk_3\big)p + rsk_2\big)\rho(k_5 + \tau_1)\gamma\Big)\beta^3 \\
& + \Big(\big(\big(k_1 r\mu + k_3(k_1 s + \mu)\big)p + \big((k_1 s + \mu)r + sk_3\big)k_2\big)(-k_4k_5 + \tau_1\tau_2)k_6 \\
& + \rho(k_5 + \tau_1)\gamma\big(\big(\mu\varphi_1 r + k_3(s\varphi_1 + \mu)\big)p + (s\varphi_1\varphi_2 + k_2\mu)r + sk_2k_3\big)\Big)\beta^2 \\
& + \Big(\big(p\mu k_1k_3 + \big(k_1 r\mu + k_3(k_1 s + \mu)\big)k_2\big)(-k_4k_5 + \tau_1\tau_2)k_6 \\
& + \rho\gamma(k_5 + \tau_1)(k_3\mu p\varphi_1 + \mu r\varphi_1\varphi_2 + s\varphi_1\varphi_2\varphi_3 + k_2k_3\mu)\Big)\beta + \mu k_1k_2k_3k_6(-k_4k_5 + \tau_1\tau_2)\Big] \\
I^* = {} & \Big[\Big(\big((p\beta^* k_3 + \beta^*(\beta^* p + \varphi_2)r + \varphi_2\varphi_3)\varphi_1 + \beta^*(\beta^* r + k_3)(\beta^* p + k_2)\big)s \\
& + \Big(\big(k_3 p + r(\beta^* p + \varphi_2)\big)\varphi_1 + (\beta^* r + k_3)(\beta^* p + k_2)\Big)\mu\Big)k_6\beta^* k_5\Lambda\Big] \\
& / \Big[-\Big(\tau_2(\beta^* + k_1)(\beta^* r + k_3)(\beta^* s + \mu)(\beta^* p + k_2)k_6 \\
& + \Big(\big((p\beta^* k_3 + \beta^*(\beta^* p + \varphi_2)r + \varphi_2\varphi_3)\varphi_1 + \beta^*(\beta^* r + k_3)(\beta^* p + k_2)\big)s \\
& + \Big(\big(k_3 p + r(\beta^* p + \varphi_2)\big)\varphi_1 + (\beta^* r + k_3)(\beta^* p + k_2)\Big)\mu\Big)\rho\beta^*\gamma\Big)\tau_1 \\
& - k_5\Big(-k_4(\beta^* + k_1)(\beta^* r + k_3)(\beta^* s + \mu)(\beta^* p + k_2)k_6 \\
& + \Big(\big((p\beta^* k_3 + \beta^*(\beta^* p + \varphi_2)r + \varphi_2\varphi_3)\varphi_1 + \beta^*(\beta^* r + k_3)(\beta^* p + k_2)\big)s \\
& + \Big(\big(k_3 p + r(\beta^* p + \varphi_2)\big)\varphi_1 + (\beta^* r + k_3)(\beta^* p + k_2)\Big)\mu\Big)\rho\beta^*\gamma\Big)\Big]
\end{aligned} \tag{5}$$

$$
\begin{aligned}
Q^* = &\Big[\Big(\big((p\beta^* k_3 + \beta^*(\beta^* p + \varphi_2)r + \varphi_2\varphi_3)\varphi_1 + \beta^*(\beta^* r + k_3)(\beta^* p + k_2)\big)s \\
&+ \Big(\big(k_3 p + r(\beta^* p + \varphi_2)\big)\varphi_1 + (\beta^* r + k_3)(\beta^* p + k_2)\Big)\mu\Big) k_6 \beta^* \tau_1 \Lambda\Big] \\
&/\Big[-\Big(\tau_2(\beta^* + k_1)(\beta^* r + k_3)(\beta^* s + \mu)(\beta^* p + k_2)k_6 \\
&+ \Big(\big((p\beta^* k_3 + \beta^*(\beta^* p + \varphi_2)r + \varphi_2\varphi_3)\varphi_1 + \beta^*(\beta^* r + k_3)(\beta^* p + k_2)\big)s \\
&+ \Big(\big(k_3 p + r(\beta^* p + \varphi_2)\big)\varphi_1 + (\beta^* r + k_3)(\beta^* p + k_2)\Big)\mu\Big)\rho\beta^*\gamma\Big)\tau_1 \\
&- k_5\Big(-k_4(\beta^* + k_1)(\beta^* r + k_3)(\beta^* s + \mu)(\beta^* p + k_2)k_6 \\
&+ \Big(\big((p\beta^* k_3 + \beta^*(\beta^* p + \varphi_2)r + \varphi_2\varphi_3)\varphi_1 + \beta^*(\beta^* r + k_3)(\beta^* p + k_2)\big)s \\
&+ \Big(\big(k_3 p + r(\beta^* p + \varphi_2)\big)\varphi_1 + (\beta^* r + k_3)(\beta^* p + k_2)\Big)\mu\Big)\rho\beta^*\gamma\Big)\Big] \\
R^* = &\Big[\Big(\Big(\big(p\beta^* k_3 + \beta^*(\beta^* p + \varphi_2)r + \varphi_2\varphi_3\big)s + \mu\big(k_3 p + r(\beta^* p + \varphi_2)\big)\Big)\varphi_1 + (\beta^* r + k_3)(\beta^* s + \mu)(\beta^* p + k_2)\Big)\beta^*(k_5 + \tau_1)\Lambda\gamma\Big] \\
&/\Big[-(\beta^* + k_1)(\beta^* r + k_3)(-k_4 k_5 + \tau_1\tau_2)(\beta^* s + \mu)(\beta^* p + k_2)k_6 \\
&- \Big(\Big(\big(p\beta^* k_3 + \beta^*(\beta^* p + \varphi_2)r + \varphi_2\varphi_3\big)s + \mu\big(k_3 p + r(\beta^* p + \varphi_2)\big)\Big)\varphi_1 + (\beta^* r + k_3)(\beta^* s + \mu)(\beta^* p + k_2)\Big)\rho\beta^*(k_5 \\
&+ \tau_1)\gamma\Big] \\
D^* = &\Big[(\tau_1 d + k_5)\beta^*\Lambda k_6\Big(\big((p\beta^* k_3 + \beta^*(\beta^* p + \varphi_2)r + \varphi_2\varphi_3)\varphi_1 + \beta^*(\beta^* r + k_3)(\beta^* p + k_2)\big)s \\
&+ \Big(\big(k_3 p + r(\beta^* p + \varphi_2)\big)\varphi_1 + (\beta^* r + k_3)(\beta^* p + k_2)\Big)\mu\Big)\zeta\Big] \\
&/\Big[-\Big(\tau_2(\beta^* + k_1)(\beta^* r + k_3)(\beta^* s + \mu)(\beta^* p + k_2)k_6 \\
&+ \Big(\big((p\beta^* k_3 + \beta^*(\beta^* p + \varphi_2)r + \varphi_2\varphi_3)\varphi_1 + \beta^*(\beta^* r + k_3)(\beta^* p + k_2)\big)s \\
&+ \Big(\big(k_3 p + r(\beta^* p + \varphi_2)\big)\varphi_1 + (\beta^* r + k_3)(\beta^* p + k_2)\Big)\mu\Big)\rho\beta^*\gamma\Big)\tau_1 \\
&+ k_5\Big(k_4(\beta^* + k_1)(\beta^* r + k_3)(\beta^* s + \mu)(\beta^* p + k_2)k_6 \\
&- \Big(\big((p\beta^* k_3 + \beta^*(\beta^* p + \varphi_2)r + \varphi_2\varphi_3)\varphi_1 + \beta^*(\beta^* r + k_3)(\beta^* p + k_2)\big)s \\
&+ \Big(\big(k_3 p + r(\beta^* p + \varphi_2)\big)\varphi_1 + (\beta^* r + k_3)(\beta^* p + k_2)\Big)\mu\Big)\rho\beta^*\gamma\Big)\Big]
\end{aligned}
$$

with $k_5 = \mu + \rho$. Furthermore, by substituting Equation (5) for Equation (4), we can obtain a non-zero equilibrium from model (1) with the equation form β^* as follows:

$$A{\beta^*}^4 + B{\beta^*}^3 + C{\beta^*}^2 + D\beta^* + E = 0, \tag{6}$$

with

$$
\begin{aligned}
A &= -prs\Big(k_6\big(k_5(\mu + \zeta) + \tau_1(d\zeta + \mu)\big) + \mu\gamma(k_5 + \tau_1)\Big), \\
B &= \Big(\Big(\Big(\big((\lambda\mu q + k_1\tau_2)\tau_1 + k_5(-k_1 k_4 + \lambda\mu)\big)k_6 + \rho\gamma\varphi_1(k_5 + \tau_1)\Big)s \\
&\quad + \big((-k_4 k_5 + \tau_1\tau_2)k_6 + \rho\gamma(k_5 + \tau_1)\big)\mu\Big)r \\
&\quad + \big((-k_4 k_5 + \tau_1\tau_2)k_6 + \rho\gamma(k_5 + \tau_1)\big)sk_3\Big)p \\
&\quad + \big((-k_4 k_5 + \tau_1\tau_2)k_6 + \rho\gamma(k_5 + \tau_1)\big)rk_2 s,
\end{aligned}
$$

$$
\begin{aligned}
C = \Big(& p\lambda r(\tau_1 q + k_5)\mu^2 \\
& + \Big(\big((\lambda\varphi_1(\tau_1 q + k_5)s + k_1(-k_4k_5 + \tau_1\tau_2)\big)r \\
& + k_3(\lambda(\tau_1 q + k_5)s + \tau_1\tau_2 - k_4k_5)\Big)p \\
& + (\lambda(\tau_1 q + k_5)s + \tau_1\tau_2 - k_4k_5)rk_2\Big)\mu \\
& + \big(pk_1k_3 + k_2(k_1 r + k_3)\big)s(-k_4k_5 + \tau_1\tau_2)\Big)k_6 \\
& + \rho\Big((k_3p\varphi_1 + r\varphi_1\varphi_2 + k_2k_3)s + \big((\varphi_1 r + k_3)p + k_2 r\big)\mu\Big)(k_5 \\
& + \tau_1)\gamma, \\
D = & \big(k_3p + r(p\varphi_1 + k_2)\big)k_6(\tau_1 q + k_5)\lambda\mu^2 \\
& + \Big(\Big(\big((p\lambda\varphi_1 qs + \lambda qsk_2 + \tau_2(k_1p + k_2)\big)\tau_1 \\
& + k_5\big(p\lambda\varphi_1 s + sk_2\lambda - k_4(k_1p + k_2)\big)\big)k_3 \\
& + \big((\lambda qs\varphi_1\varphi_2 + k_1k_2\tau_2)\tau_1 + k_5(\lambda\varphi_1\varphi_2 s - k_1k_2k_4)\big)r\Big)k_6 \\
& + \rho\gamma(k_5 + \tau_1)\big((p\varphi_1 + k_2)k_3 + r\varphi_1\varphi_2\big)\Big)\mu \\
& + \big(k_1k_2(-k_4k_5 + \tau_1\tau_2)k_6k_3 + \rho\gamma\varphi_1\varphi_2\varphi_3(k_5 + \tau_1)\big)s, \\
E = & \hat{E}(1 - \mathcal{R}_0),
\end{aligned}
$$

with $\hat{E} = -\mu k_1k_2k_3k_6\big(k_5(\gamma + \mu + \zeta) + \tau_1(d\zeta + \gamma + \mu)\big)$.

The polynomial Equation (6) can be analyzed to determine the chance of endemic equilibrium in the model. Remember that the values of A and $\hat{E}$ are always negative. The following theorems are obtained when the values B, C, and D are positive or negative and $\mathcal{R}_0$ is less than or greater than one:

Theorem 1. *The Model (1) has*

(i) a unique endemic equilibrium if $E > 0$, which occurs iff $\mathcal{R}_0 > 1$, provided that one of the following conditions is met:
   - *a) the coefficients B, C, and D are either all positive or all negative,*
   - *b) B is negative, D is positive, and C may be either positive or negative.*

(ii) two endemic equilibria when $E < 0$, a condition that holds true iff $\mathcal{R}_0 < 1$, provided that one of the following conditions is met:
   - *a) both B and C are positive, whereas D may be either positive or negative,*
   - *b) coefficients C and D may both be positive or negative, whereas variable B is always the inverse sign,*
   - *c) B with either C or D being negative, and the other coefficient is positive.*

(iii) three endemic equilibria when $E > 0$ iff $\mathcal{R}_0 > 1$, provided that one of the following conditions is met:
   - *a) B, with either C or D being positive and the other coefficient being negative,*
   - *b) D with B or C negative and the other coefficient positive.*

(iv) four endemic equilibria when $E < 0$ iff $\mathcal{R}_0 < 1$, and the coefficients B and D are positive, whereas C is negative.

(v) no endemic equilibrium otherwise.

Furthermore, we will explore the behavior of bifurcation on the model. First, let $\mathbf{x} = (x_1, x_2, x_3, x_4, x_5, x_6, x_7, x_8)^T = (S, V_1, V_2, V_3, I, Q, R, D)^T$. Therefore, the model can be rewritten in the form $\frac{dx}{dt} = f(x)$, with $f(x) = \big(f_1(x), \ldots, f_8(x)\big)$, as follows:

$$
\begin{aligned}
x_1' &= \Lambda - \frac{\lambda x_1 x_5}{N} - \frac{\lambda q x_1 x_6}{N} - \varphi_1 x_1 + \rho x_7 - \mu x_1 = f_1,\\
x_2' &= \varphi_1 x_1 - \frac{\lambda p x_2 x_5}{N} - \frac{\lambda p q x_2 x_6}{N} - \varphi_2 x_2 - \mu x_2 = f_2,\\
x_3' &= \varphi_2 x_2 - \frac{\lambda r x_3 x_5}{N} - \frac{\lambda r q x_3 x_6}{N} - \varphi_3 x_3 - \mu x_3 = f_3,\\
x_4' &= \varphi_3 x_3 - \frac{\lambda s x_4 x_5}{N} - \frac{\lambda s q x_4 x_6}{N} - \mu x_4 = f_4,\\
x_5' &= \frac{\lambda x_1 x_5}{N} + \frac{\lambda p x_2 x_5}{N} + \frac{\lambda r x_3 x_5}{N} + \frac{\lambda s x_4 x_5}{N} + \frac{\lambda q x_1 x_6}{N} + \frac{\lambda p q x_2 x_6}{N} + \frac{\lambda r q x_3 x_6}{N}\\
&\qquad + \frac{\lambda s q x_4 x_6}{N} - \tau_1 x_5 + \tau_2 x_6 - \gamma x_5 - \zeta x_5 - \mu x_5 = f_5,\\
x_6' &= \tau_1 x_5 - \tau_2 x_6 - \gamma x_6 - \zeta d x_6 - \mu x_6 = f_6,\\
x_7' &= \gamma x_5 + \gamma x_6 - \rho x_7 - \mu x_7 = f_7,\\
x_8' &= \zeta x_5 + \zeta d x_6 = f_8,\\
N &= x_1 + x_2 + x_3 + x_4 + x_5 + x_6 + x_7 + x_8.
\end{aligned}
\tag{7}
$$

Then choose λ as the bifurcation parameter with E^0 as the disease-free equilibrium point. After that the model (1) can undergo bifurcation at $\mathcal{R}_0 = 1$, then $\lambda^* = \lambda = \frac{k_1\big((\tau_1+k_5)\mu+(d\zeta+\gamma)\tau_1+k_5(\gamma+\zeta)\big)k_3k_2}{(q\tau_1+k_5)\Big(\big((k_3p+r\varphi_2)\varphi_1+k_2k_3\big)\mu+s\varphi_1\varphi_2\varphi_3\Big)}$. The Jacobian Matrix of the system (7) at E^0 and evaluated for $\lambda = \lambda^*$ is given as,

$$
\mathbf{J}(E^0, \lambda^*) = \begin{bmatrix}
-k_1 & 0 & 0 & 0 & -\frac{\lambda\mu}{k_1} & -\frac{\lambda q\mu}{k_1} & \rho & 0\\
\varphi_1 & -k_2 & 0 & 0 & -\frac{\mu\varphi_1 p\lambda}{k_1k_2} & -\frac{\mu\varphi_1 qp\lambda}{k_1k_2} & 0 & 0\\
0 & \varphi_2 & -k_3 & 0 & -\frac{\lambda\varphi_2\mu r\varphi_1}{k_1k_2k_3} & -\frac{\mu\varphi_1\varphi_2 qr\lambda}{k_1k_2k_3} & 0 & 0\\
0 & 0 & \varphi_3 & -\mu & -\frac{\varphi_1\varphi_2\varphi_3 s\lambda}{k_1k_2k_3} & -\frac{\lambda sq\varphi_3\varphi_2\varphi_1}{k_1k_2k_3} & 0 & 0\\
0 & 0 & 0 & 0 & \frac{K_1}{\big((\varphi_2+k_3)\mu+\varphi_2\varphi_3\big)\varphi_1+k_2k_3\mu} & \frac{K_2}{\big((\varphi_2+k_3)\mu+\varphi_2\varphi_3\big)\varphi_1+k_2k_3\mu} & 0 & 0\\
0 & 0 & 0 & 0 & \tau_1 & -k_5 & 0 & 0\\
0 & 0 & 0 & 0 & \gamma & \gamma & -k_6 & 0\\
0 & 0 & 0 & 0 & \zeta & d\zeta & 0 & 0
\end{bmatrix}
$$

with $K_1 = \Big(\big((\lambda r - k_4)\varphi_2 + k_3(\lambda p - k_4)\big)\mu + \varphi_2\varphi_3(\lambda s - k_4)\Big)\varphi_1 + k_2k_3\mu(\lambda - k_4)$ and $K_2 = \Big(\big((\lambda qr + \tau_2)\varphi_2 + k_3(\lambda pq + \tau_2)\big)\mu + \varphi_2\varphi_3(\lambda qs + \tau_2)\Big)\varphi_1 + k_2k_3\mu(\lambda q + \tau_2)$.

The Jacobian Matrix of system (7) has a zero-part eigenvalue and has all negative parts of the other eigenvalues. As a result, we applied the center manifold theorem to analyze behavior near $\lambda = \lambda^*$.

Furthermore, let $\mathbf{v} = (v_1, v_2, v_3, v_4, v_5, v_6, v_7, v_8)$ be the left eigenvector of the Jacobian Matrix $\mathbf{J}(E^0, \lambda^*)$ corresponding to the zero real part eigenvalue. Then we get $\mathbf{v}$ as follows:

$$\begin{aligned} &v_1 = 0, v_2 = 0, v_3 = 0, v_4 = 0, \\ &v_5 = -\frac{\zeta(d\tau_1 + k_5)(k_2k_3\mu + k_3\varphi_1\mu + \varphi_1\varphi_2\mu + \varphi_1\varphi_2\varphi_3)}{K_1k_5 + K_2\tau_1}v_8, \\ &v_6 = \frac{\zeta(K_1d - K_2)}{K_1k_5 + K_2\tau_1}v_8, v_7 = 0, v_8 = v_8 \end{aligned} \tag{8}$$

From the Jacobian Matrix $\mathbf{J}(E^0, \lambda^*)$, we obtained the right eigenvector corresponding to $\mathbf{v} \cdot \mathbf{w} = 1$. Let $\mathbf{w} = (w_1, w_2, w_3, w_4, w_5, w_6, w_7, w_8)$, then

$$\begin{aligned} &w_1 = 0, w_2 = 0, w_3 = 0, w_4 = 0, \\ &w_5 = -\frac{K_1k_5 + K_2\tau_1}{2\zeta(k_5 + d\tau_1)\left(\left((k_3 + \varphi_2)\mu + \varphi_2\varphi_3\right)\varphi_1 + k_2k_3\mu\right)}, \\ &w_6 = \frac{K_1k_5 + K_2\tau_1}{2\zeta(K_1d - K_2)}, w_7 = 0, w_8 = 0 \end{aligned} \tag{9}$$

Furthermore, we defined coefficients $\hat{a}$ and $\hat{b}$ using the Theorem of Castillo-Chavez and Song [16] as follows:

$$\hat{a} = \sum_{k,i,j=1}^{8} v_k w_i w_j \frac{\partial^2 f_k}{\partial x_i \partial x_j}(E_0, \lambda^*),$$
$$\hat{b} = \sum_{k,i=1}^{8} v_k w_i \frac{\partial^2 f_k}{\partial x_i \partial \lambda}(E_0, \lambda^*).$$

Considering the values of Equations (8) and (9), we get

$$\hat{a} = \frac{\psi_1\psi_2\lambda k_2(K_1k_5 + K_2\tau_1)\left(\left((k_3p + r\varphi_2)\varphi_1 + k_2k_3\right)\mu + s\varphi_3\varphi_2\varphi_1\right)k_1k_3\mu}{2\left(\left((\varphi_2 + k_3)\varphi_1 + k_2k_3\right)\mu + \varphi_1\varphi_2\varphi_3\right)^3(K_1d - K_2)^2\Lambda\zeta(d\tau_1 + k_5)} \tag{10}$$

$$\hat{b} = \frac{\psi_1\left(\left((k_3p + r\varphi_2)\mu + s\varphi_2\varphi_3\right)\varphi_1 + k_2k_3\mu\right)}{2(K_1d - K_2)\left(\left((\varphi_2 + k_3)\mu + \varphi_2\varphi_3\right)\varphi_1 + k_2k_3\mu\right)} \tag{11}$$

with

$$\psi_1 = \left(-\left((\varphi_2 + k_3)\varphi_1 + k_2k_3\right)q(d\tau_1 + k_5)\mu - \varphi_2\varphi_3q(d\tau_1 + k_5)\varphi_1 + K_1d - K_2\right)$$
$$\psi_2 = \left(-\left((\varphi_2 + k_3)\varphi_1 + k_2k_3\right)(d\tau_1 + k_5)\mu - \varphi_2\varphi_3(d\tau_1 + k_5)\varphi_1 + K_1d - K_2\right).$$

According to the Castillo-Chavez and Song theorem [16], backward bifurcation takes place when both coefficients $\hat{a}$ and $\hat{b}$ are positive. Therefore, our next step will be to identify the conditions under which these coefficients can be positive. We will focus on the components of coefficients $\hat{a}$ and $\hat{b}$ that may influence their sign, specifically $K_1d - K_2$, $K_1k_5 + K_2\tau_1$, ψ_1, and ψ_2. First, consider the value $K_1d - K_2$, which can be positive or negative.

$$\lambda < \frac{\left(\left((\varphi_2 + k_3)\mu + \varphi_2\varphi_3\right)\varphi_1 + k_2k_3\mu\right)(dk_4 + \tau_2)}{\left(\left((k_3p + r\varphi_2)\mu + s\varphi_2\varphi_3\right)\varphi_1 + k_2k_3\mu\right)(d - q)} \tag{12}$$

If the inequality (12) holds, $K_1d - K_2$ will be negative. This ensures that the denominator, $\hat{b}$, is negative. After checking the numerator of $\hat{b}$, there is ψ_1, which will be negative in this case, resulting in a negative numerator for $\hat{b}$. As a result, the coefficient for $\hat{b}$ is positive. The coefficient $\hat{a}$ in the negative $K_1d - K_2$ scenario is squared in the denominator $\hat{a}$, ensuring a positive denominator. Next, for the numerator $\hat{a}$ involving ψ_1 and ψ_2, negative values $K_1d - K_2$ imply that ψ_1 and ψ_2 are negative, so we only need to check $K_1k_5 + K_2\tau_1$, which can be positive or negative. If the inequality (13), which comes from $K_1k_5 + K_2\tau_1$, is satisfied, the numerator $\hat{a}$ is positive, and thus the coefficient $\hat{a}$ is positive. As a result, the system will undergo backward bifurcation.

$$\lambda > \frac{\left(\left((\varphi_2 + k_3)\mu + \varphi_2\varphi_3\right)\varphi_1 + k_2k_3\mu\right)\left(k_5(\gamma + \mu + \zeta) + \tau_1(d\zeta + \gamma + \mu)\right)}{(q\tau_1 + k_5)\left(\left((k_3p + r\varphi_2)\mu + \varphi_2\varphi_3s\right)\varphi_1 + k_2k_3\mu\right)} \tag{13}$$

In the case where the inequality (12) is not met or the value $K_1d - K_2$ is positive, it is easier to ensure that the denominators of these two coefficients are positive.

$$\lambda > \frac{\left((q\tau_1 + k_4)d + qk_5 + \tau_2\right)\left(\left((\varphi_2 + k_3)\mu + \varphi_2\varphi_3\right)\varphi_1 + k_2k_3\mu\right)}{\left(\left((k_3p + r\varphi_2)\mu + \varphi_2\varphi_3s\right)\varphi_1 + k_2k_3\mu\right)(d - q)} \tag{14}$$

The inequalities (14) and (15) derive from ψ_1 and ψ_2, respectively. First, we will look at the coefficient $\hat{b}$. If the inequality (14) is not satisfied, the numerator $\hat{b}$ becomes negative, which leads to forward bifurcation. However, if the inequality (14) is true, the coefficient $\hat{b}$ must be positive. This allows us to proceed to the coefficients $\hat{a}$. When evaluating the numerator of the coefficient $\hat{a}$, consider the value ψ_2 and the form $K_1k_5 + K_2\tau_1$.

$$\lambda > \frac{\left((\tau_1 + k_4)d + \tau_2 + k_5\right)\left(\left((\varphi_2 + k_3)\mu + \varphi_2\varphi_3\right)\varphi_1 + k_2k_3\mu\right)}{\left(\left((k_3p + r\varphi_2)\mu + \varphi_2\varphi_3s\right)\varphi_1 + k_2k_3\mu\right)(d - q)} \tag{15}$$

It is important to consider the inequalities (13) and (15). If both inequalities are satisfied, the coefficient $\hat{a}$ will be positive, meaning a backward bifurcation of the system occurs.

Based on the previous discussion, we can obtain the following theorem:

Theorem 2. *Model* (1) *will undergo a backward bifurcation at* $\mathcal{R}_0 = 1$ *if either inequalities* (12) *and* (13) *are met, or inequalities* (13)–(15) *are concurrently satisfied.*

The endemic equilibrium of model (1) is obtained by solving the β^* equation. Next, using Equation (6), we can determine all positive solutions along the bifurcation parameter ($\mathcal{R}_0$). Hence, we can obtain the bifurcation diagram of system 1 in each phase. Theorems 1 and 2 will then be used to characterize system dynamics in the phase following the giving of booster vaccinations to the population.

Table 5 shows that the coefficients A, B, C, D, and $\hat{E}$ are all negative. After checking Theorem 1, it is clear that in the post-booster vaccination phase, the system exhibits a unique endemic equilibrium when $\mathcal{R}_0 > 1$ and no endemic equilibrium when $\mathcal{R}_0 < 1$. This trend indicates that the system is moving toward forward bifurcation. To confirm this, Theorem 2 can be used. From columns 8–11 in **Table 5**, it shows that none of the inequalities are met during the post-vaccine booster phase. As a result, Theorem 2 states that the system will bifurcate forward. The presence of forward bifurcation indicates that this system is easier to control than systems with backward bifurcation. This is because smooth changes in stable equilibrium conditions can occur without causing sudden stability changes. To be more precise, we will attempt to model the system bifurcation diagram for each phase. **Figure 1** depicts the simulation results for each phase of the bifurcation diagram.

Table 5. The values A, B, C, D, $\hat{E}$, and the right hand side of inequalities (12)–(15) in the phase after booster vaccination.

Phase	A	B	C	D	$\hat{E}$	λ	Right hand side of inequality			
							(12)	(13)	(14)	(15)
4	-4.7×10^{-7}	-1.4×10^{-7}	-6×10^{-9}	-6.9×10^{-11}	-1.5×10^{-13}	0.401	−0.5	0.406	−0.6	−2.3
5	-4.5×10^{-9}	-1.4×10^{-10}	-1.1×10^{-12}	-3.1×10^{-15}	-7.4×10^{-18}	0.018	−0.12	0.03	−0.15	−0.77
6	-1.1×10^{-8}	-4.1×10^{-9}	-1×10^{-10}	-5.9×10^{-13}	-8.9×10^{-16}	0.017	−0.13	0.04	−0.15	−0.5

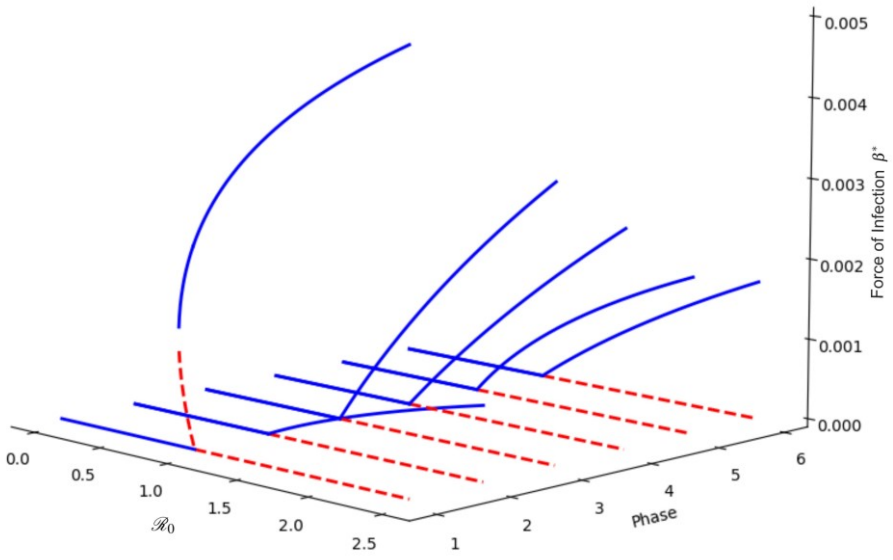

Figure 1. Bifurcation diagram.

Figure 1 shows simulation results of bifurcation diagrams for different phases, showing various bifurcation behaviors. The early phase is distinguished by a backward bifurcation pattern, indicating a more difficult disease control situation. This is due to a sudden increase in the stable equilibrium indicated by the force of infection values, particularly near the basic reproduction number ($\mathcal{R}_0$) of 1. In contrast, the next phase exhibits forward bifurcation, indicating a more controllable system. In this phase, changes in stability at the equilibrium point are predictable, and secondary infection rates greater than one do not result in an explosion of cases like in the first phase.

Next, we will look at the values obtained in each phase. When we examine the dynamics of total infection cases in a population, we can see that phases 1 and 3 saw an increase in cases, which was associated with increased population mobility. This is reflected in the bifurcation diagram, which shows higher values for these phases than other phases. The bifurcation diagram in phase 2 shows a shift from backward to forward and a significant decrease in the peak point $\mathcal{R}_0$ from phase 1. This indicates the impact of giving the two-dose vaccine. Finally, we observed conditions following the distribution of the booster vaccine to the public. The bifurcation diagrams for phases 4, 5, and 6 all show controlled conditions, as indicated by changes in the maximum value of $\mathcal{R}_0$ becoming lower. For instance, with $\mathcal{R}_0$ of 2.5, the value of β^* in phase 5 is 0.00193, and in phase 6, it is 0.00171. These changes suggest that giving additional vaccine doses can alter system dynamics, resulting in more controlled conditions. In practice, this means that any sudden increase in cases or secondary infections in a population will result in fewer severe cases than if no booster vaccine dose was given.

3.4. Sensitivity analysis

Sensitivity analysis of $\mathcal{R}_0$ was conducted to identify the parameters that could provide the most significant changes to $\mathcal{R}_0$. Sensitivity analysis of the parameter values in phase 6 was performed. Then, as shown in **Table 6**, the sensitivity index of each parameter was obtained.

Table 6. Parameter sensitivity index.

Parameters	Phase 6 Sensitivity Index	Parameters	Phase 6 Sensitivity Index
λ	1	φ_1	-3.349×10^{-5}
τ_1	−0.368	r	6.385×10^{-6}
ζ	−0.353	φ_3	-5.27×10^{-7}
γ	−0.327	s	2.287×10^{-7}
q	0.155	p	1.177×10^{-7}
τ_2	0.103	φ_2	-8.434×10^{-8}
μ	−0.055	ρ	-8.434×10^{-8}
d	−0.012		

Table 6 shows the sensitivity levels of the parameters, sorted from most sensitive to least sensitive. The parameters most sensitive to $\mathcal{R}_0$ include the rate of infection (λ), the rate of movement from $I(t)$ to $Q(t)$ (τ_1), the rate of COVID-19 mortality (ζ), and the rate of recovery (γ).

3.5. Numerical simulation

Numerical simulations were conducted to further explore the behavior of the system. The simulation was performed on a system with conditions such as those in phase 6. Hence, the estimated parameter values from phase 6 were used. First, we looked at the bifurcation diagram produced in the 6th phase. As shown in **Figure 1**, the system in phase 6 undergoes the forward bifurcation that was interpreted

previously. Now, we can further examine what happens when the system in this phase experiences backward bifurcation.

Based on the sensitivity analysis that was conducted previously, the parameter λ was the most sensitive to changes in $\mathcal{R}_0$. Next, variations in the λ value will be performed to obtain backward bifurcation in the system in phase 6. To accomplish this, we will use the conditions outlined in Theorem 2, which will guide modifications in λ to ensure the system transitions to the backward bifurcation state.

When selecting a parameter other than λ to explore backward bifurcation, it is essential to use a sufficiently large value. This necessity arises because λ is the parameter that significantly influences the development of backward bifurcation. A sensitivity value for λ approaching 1 suggests that even minor changes in this parameter can lead to substantial alterations in the system's dynamics. Conversely, the sensitivity values of other parameters in the model are generally below 0.5, with some being exceedingly low, nearing 0. This indicates that variations in these other parameters will have minimal impact on the system's behavior, particularly regarding the formation of backward bifurcation. Therefore, λ emerges as the pivotal parameter determining the occurrence of backward bifurcation in the model and thus becomes the primary focus of analysis and simulation aimed at understanding the dynamics of disease spread. We will begin by simulating the bifurcation of the system when λ equals 2.

If we looked at the backward bifurcation in **Figure 2**, the change in the equilibrium of the system from secondary infection from the left to the right, when the value $\mathcal{R}_0 = 1$ arrives, a backward bifurcation occurs. The equilibrium of the system, which previously had a value of 1, namely the disease-free equilibrium, in the range $0.839 < \mathcal{R}_0 < 1$ has three equilibria (two stable equilibria and one unstable equilibrium). Furthermore, if changes occur again when $\mathcal{R}_0 > 1$, the equilibrium of the system becomes two (an unstable disease-free equilibrium and a stable endemic equilibrium). We need to pay attention when the secondary infection value moves to > 0, at this point, there is a change in the endemic equilibrium value, which suddenly increases to a value of 0.00256. This is extremely different from forward bifurcation where endemic equilibrium changes occur gradually. Thus, during backward bifurcation, there could be a sudden increase in the number of cases if secondary infections in the system have exceeded number 1. As a result, standard medical interventions against COVID-19 will become more challenging due to the increase in the number of cases in the system.

To make it clearer, we looked at the bifurcation diagram between secondary infection parameters and compartment I^*. As depicted in **Figure 3**, we identified the change in the system's equilibrium when it passes secondary infection 1. The backward bifurcation produced by the system in phase 6 causes an endemic equilibrium, which immediately jumps to 5.3 million until the secondary infection value reaches the endemic equilibrium point for compartment I^* at 6.8 million. This was extremely different from forward bifurcation in a system where the endemic equilibrium point gradually increases. That is, at the endpoint, secondary infections in the diagram are only at 4.4 million. This difference could explain why a system with backward bifurcation experiences more difficulties in controlling disease transmission

with standard interventions because there was an extremely high increase in the number of cases compared with a system with forward bifurcation. On the other hand, forward bifurcation made it possible to implement efficient medical interventions that might lessen or even reverse the trend, possibly leading to the system's return to a state free of disease.

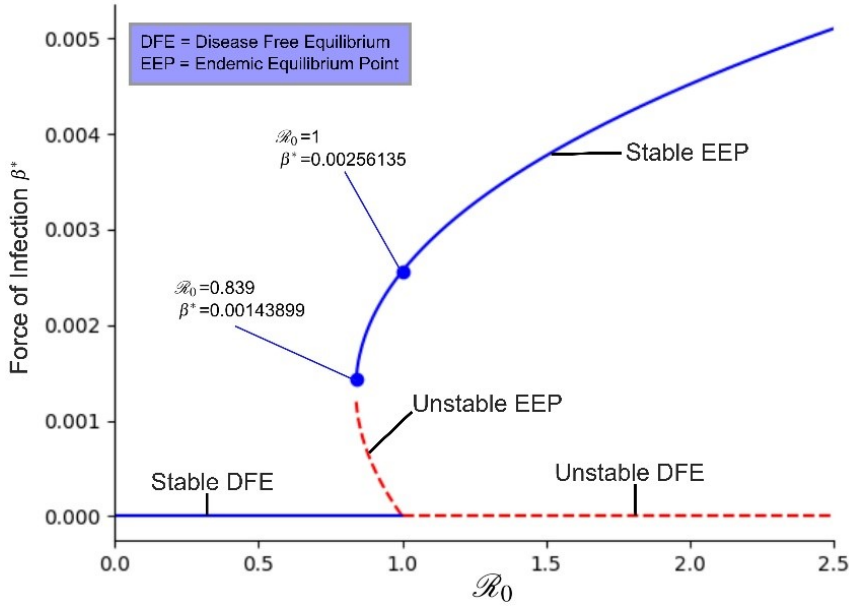

Figure 2. Backward bifurcation of the system in phase 6 with variation of λ.

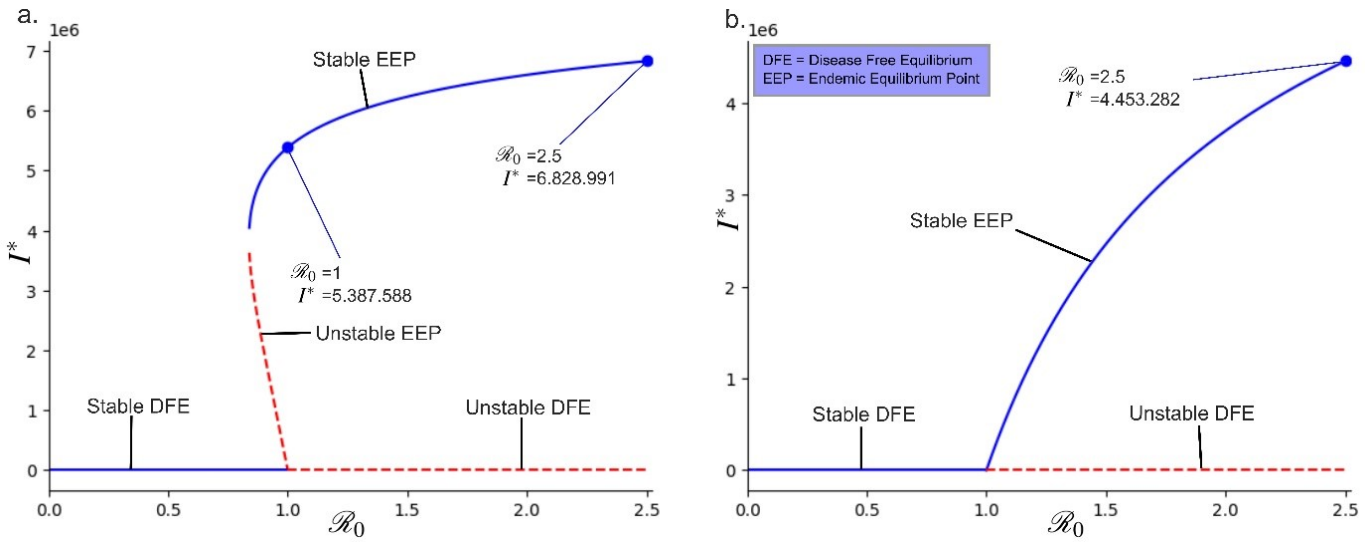

Figure 3. Backward bifurcation **(a)** and forward bifurcation **(b)** in a phase 6.

On the other hand, bifurcation simulations that varied the value of λ revealed that a progressive increase in λ leads to a shift in the system's behavior from forward bifurcation to backward bifurcation. This phenomenon suggests that a continuous rise in λ can exacerbate conditions for disease spread within the system. One significant drawback of backward bifurcation is the challenge it poses for implementing effective disease mitigation or management strategies. In this scenario, even if the basic reproduction number is reduced below one, the disease can still persist at a notable

endemic level. Consequently, control measures that are typically effective during forward bifurcation may prove insufficient, necessitating more intensive and sustained interventions to manage the disease spread. Therefore, the findings of this simulation underscore the critical need to monitor and regulate the value of λ in efforts to prevent and mitigate disease transmission.

Then, we could simulate several compartments in the system to identify the system's behavior. Previously, we could first look for the herd immunity threshold value in the system with $HIT = \left(1 - \frac{1}{\mathcal{R}_0}\right) \times \frac{1}{\text{VaccineEfficacy}}$ [27]. Vaccine efficacy with a value of 95% with the highest secondary infection value from the phase in the system can provide a threshold for herd immunity from the system of 68% or around 189 million people who must be, at least, immune to COVID-19 to achieve herd immunity. Next, we could look at the simulation of compartments $I(t)$ and $Q(t)$ in the system up to day 1800.

According to the simulation results in **Figure 4**, each compartment did not reach the predetermined HIT limit. However, based on the simulation results up to day 1800, the behavior of the system compartments was converging to one point.

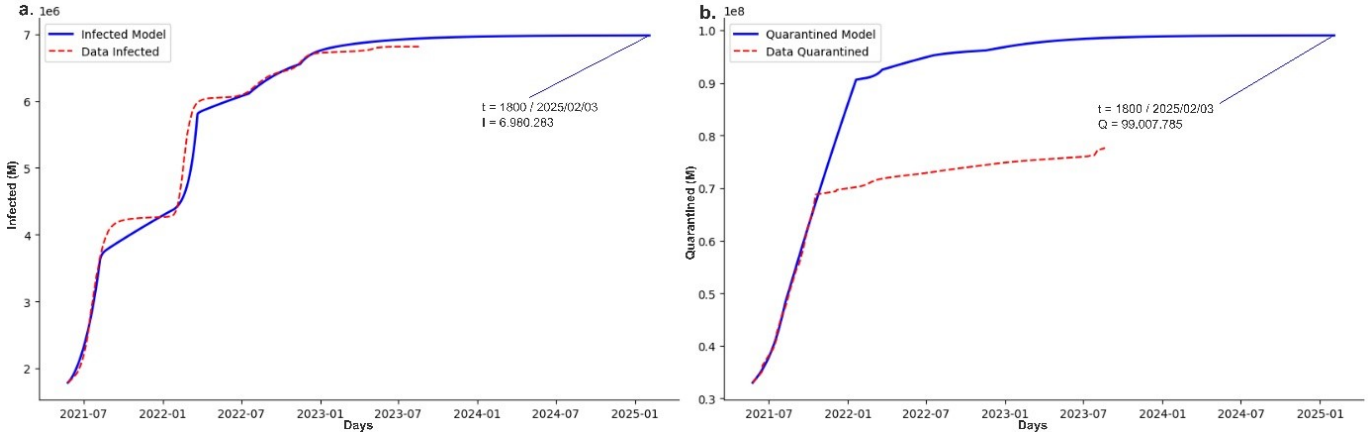

Figure 4. Simulation of the cumulative value of compartments $I(t)$ and $Q(t)$.

Next, we expanded the simulation to include more compartments, continuing until the desired herd immunity threshold was met. Our attention will shift to the First Dose Vaccine $\left(V_1(t)\right)$ compartment, recognizing that herd immunity can be achieved through both natural infection and medical interventions such as vaccination. This approach allows for the development of individual immunity within the population. The simulation will take place in the First Dose Vaccine $\left(V_1(t)\right)$ compartment until day 1800.

Figure 5 shows the state of the system after exceeding the herd immunity threshold (HIT). Following HIT, there was a convergence trend, with the administration of 246 million vaccine doses. This trend corresponds to expected outcomes in a real-world scenario in which herd immunity is achieved, as evidenced by low levels of infection while the disease persists, resulting in consistent case numbers and ongoing vaccination efforts. The infection and quarantine compartments show similar trends of stability and convergence. Based on the model simulation analysis, it was discovered that the system begins in phase 6, which leads to herd

immunity. This development is distinguished by the stabilization of infection cases and the achievement of values that exceed the herd immunity threshold, which has been established in the support compartment to achieve herd immunity.

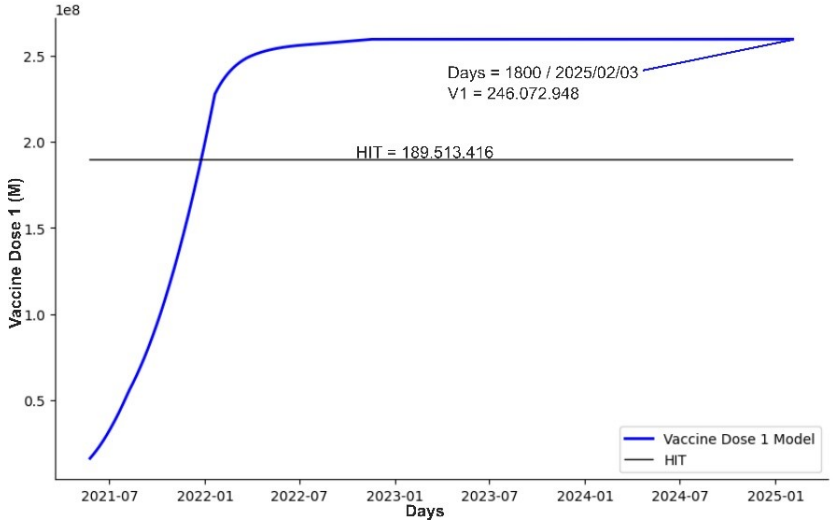

Figure 5. Simulation of the initial vaccination dose compartment $V_1(t)$ within a system.

Model simulations over time indicate that the system may have achieved herd immunity. To better understand how herd immunity works in the system under study, we will use additional tools at our disposal. Let us first consider the impact on a population once herd immunity is established. Herd immunity makes it difficult for disease-causing pathogens to infect susceptible individuals via contact within the population. When the majority of the population is immune to a pathogen, the number of susceptible individuals decreases, resulting in reduced or stopped transmission [28]. Next, focus on the secondary infection value ($\mathcal{R}_0$) and the bifurcation diagram in phase 6, as shown in **Figure 6**. We find that the secondary infection value ($\mathcal{R}_0$) is within the disease-free equilibrium zone. This indicates a stable situation without an epidemic. Secondary infection values ($\mathcal{R}_0$) below one indicates a gradual decline in the epidemic, potentially leading to its disappearance from the population. In contrast, a secondary infection ($\mathcal{R}_0$) value above zero but less than one indicates that, while the outbreak may subside, the disease, in this case COVID-19, may persist in the population indefinitely. Herd immunity dynamics are reflected in the secondary infection value ($\mathcal{R}_0$) and its bifurcation, which show characteristics consistent with this phenomenon. Thus, we conclude that the system, particularly in phase 6, has the potential to achieve herd immunity.

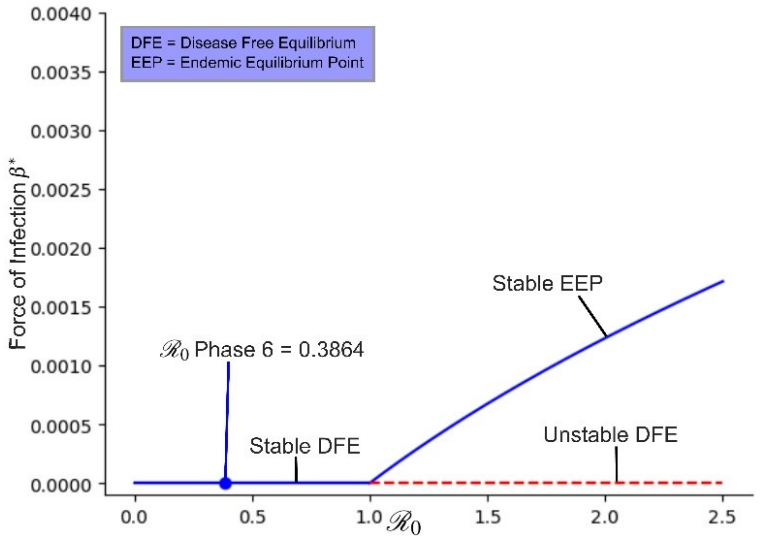

Figure 6. Bifurcation diagram and secondary infection value ($\mathcal{R}_0$) of the system in phase 6.

In addition to presenting numerical simulations of daily total cases, the upcoming simulation will concentrate on daily COVID-19 infection cases. This simulation aims to provide a more nuanced understanding of the day-to-day dynamics of disease transmission. By visualizing daily infection cases, we can closely observe the fluctuations and patterns of the spread, identify peaks and troughs, and assess the effectiveness of interventions such as quarantine measures and vaccination efforts. This information is vital for comprehending the speed of virus transmission, forecasting potential surges in cases, and developing more adaptable control strategies.

3.6. Discussion

The results from the numerical simulations reveal significant changes in the system's dynamics in response to variations in the parameter λ, which denotes the infection rate. At lower values of λ, the system demonstrates forward bifurcation characteristics typical of an epidemiological model, where the rise in cases occurs gradually and in a controlled manner. This indicates a scenario where the disease spreads slowly, allowing for effective interventions such as quarantine and vaccination to contain its spread.

However, as λ increases, the system transitions toward backward bifurcation. In this phase, the escalation in the infection rate leads to a sharp and rapid spike in cases, followed by a similarly steep decline. This change in bifurcation behavior highlights the model's sensitivity to the infection rate, underscoring the critical need to regulate λ to prevent uncontrolled surges in cases. These findings suggest that in environments with a high infection rate, intervention strategies must be more aggressive and prompter to avert entering the backward bifurcation phase, where control becomes significantly more challenging.

The results from the numerical simulations of total disease cases provide a complex understanding of herd immunity. Traditionally, herd immunity is defined by the percentage of the population that has immunity-either through natural infection or vaccination-needed to halt the spread of the disease. In this simulation, even though

the total cumulative cases of infection and quarantine have not yet reached the herd immunity threshold, the compartment for individuals who received the first dose of vaccination shows a significant level of immunity that exceeds the estimated required threshold. This suggests that vaccination may have established an effective immune barrier within the population.

Furthermore, the analysis of the system's $\mathcal{R}_0$ value, which is in the disease-free endemic area, provides additional support for the claim of herd immunity. A low $\mathcal{R}_0$ indicates that each infection case results in less than one new case, which is characteristic of herd immunity conditions. Additionally, it should be considered that herd immunity is not just about reaching a certain percentage, but also about the distribution of immunity within the population. In this simulation, widespread vaccination may have created a more even distribution of immunity, which is effective in protecting vulnerable groups and reducing the spread of the disease. Thus, although the herd immunity threshold metrics may not have been fully met, the combination of high vaccination rates, low $\mathcal{R}_0$ values, and effective immune distribution indicates that the system has achieved a functional level of herd immunity.

In **Figure 4**, we can observe a unique pattern in the system. In the first and third phases, there is a high increase in the number of cases. Then, in the remaining phase, the increase in the number of cases was not high. We first concentrate on the λ values in phases 1 and 3. The estimation results might not have been totally credible, as evidenced by the fact that phase 1, despite having the highest increase, had a lower infection rate than phase 3 when compared to the simulation shown in **Figure 4**. In addition, the infection rate (λ) in phase 4 was surprisingly higher than in phases 1 and 3. In order to go further, we would then look at the system's simulation of daily infection cases.

As shown in **Figure 7**, the highest spike was in phase 3. Furthermore, there was a low spike in the cumulative cases in phase 3 compared with that in phase 1. This finding could be attributed to the fact that the duration in phase 3 was shorter than that in phase 1. Then, we attempted to evaluate the reasons behind the high peak point of daily cases in phase 3 and why phase 3 was shorter than phase 1.

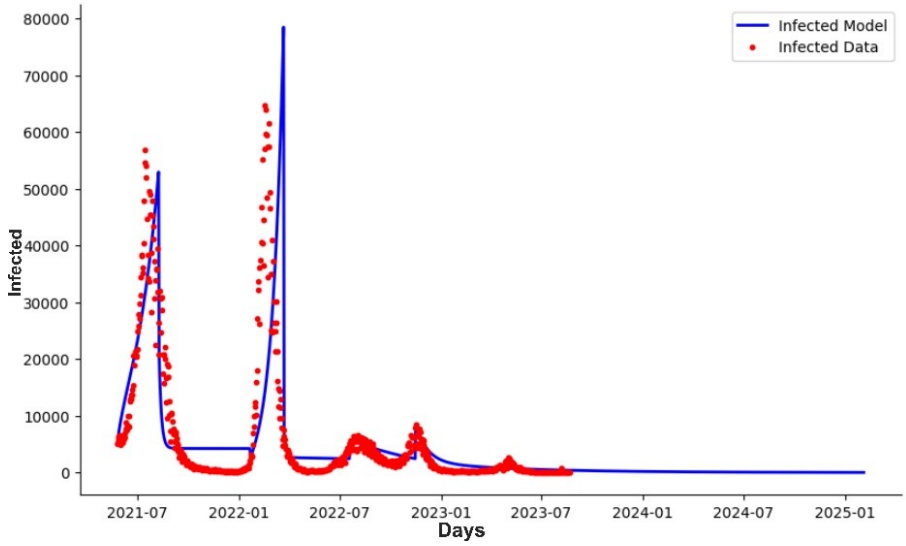

Figure 7. $I(t)$ distribution for daily cases.

According to the estimation results (**Table 3**), the value of τ_1, which was the rate of movement from compartment $I(t)$ to $Q(t)$ in phase 3, was smaller than the infection rate. This condition was reversed to the condition in phase 1. Therefore, the number of people who tested positive and who are quarantined in phase 3 was fewer compared with that in phase 1. If there were fewer individuals quarantined, then the number would be greater in other phases during an explosion of daily cases. Next, we paid attention to the estimation results of γ or recovery rate. γ in phase 3 is slightly greater than that in phase 1. This indicated that more people recovered quickly from the outbreak in phase 3 compared with phase 1. Therefore, this result indicated the achievement of group immunity. The conditions in phase 3, which included a high daily rate of infection cases and a faster recovery rate, provided reasons why this phase occurred more quickly than phase 1. That is, the cumulative cases in phase 3 were more likely to be lower than that in phase 1.

As we enter phase 4, we find that λ has the highest infection rate. The Phase 4 results show a significant λ, which correlates with a significant τ_1 value. This implies that strict quarantine regulations were implemented during this phase, effectively reducing the number of infection cases in the community. In contrast, a spike in cases occurs when τ_1 exceeds λ in phase 1. This difference could be attributed to the lower recovery rate in phase 1 compared to phase 4. The early phase of vaccination interventions, which has not yet had a significant impact on the population, adds to the explanation for the early phase peak. In contrast, Phase 4 includes intensive vaccination campaigns and booster vaccinations, which makes sense because it improves recovery rates and reduces the number of people at risk of infection following vaccination.

Finally, we conclude that the roles of λ, γ, and τ_1 are interrelated with the epidemic in the system. Balancing parameter values in the system, particularly the three parameters discussed previously, controlled the spread of the outbreak in the system. With a controlled system, forward bifurcation in the system can be achieved. Hence, it is easier to control secondary infections. Therefore, disease transmission in a controlled system also supports the achievement of herd immunity in a specific population.

Based on the numerical simulations obtained, we will compare them with an intriguing approach to disease spread modeling. Kyurkchiev [29] is developing a model that uses the infection rate and other parameters as polynomial functions, offering flexibility for complex disease dynamics. However, this complexity may complicate interpretation and analysis.

In contrast, the epidemiological model used in this study incorporates simpler parameters through vaccination and quarantine interventions. We effectively captured disease dynamics by partitioning the data according to its trends, demonstrating that flexibility does not require complex parameters. By understanding trends and partitioning accurately, we achieved reliable results with a simpler model.

Kyurkchiev's approach [29] may better suit diseases with complex dynamics and rapid parameter changes, while our model fits diseases with more stable trends where interventions significantly impact outcomes. It is crucial to balance flexibility and interpretability. Although complex models may provide more accurate results, they

can be harder to interpret. Simpler models, while potentially less accurate, are easier to understand and communicate to policymakers and the public, emphasizing the need to consider accuracy alongside usability in model selection.

The COVID-19 epidemic model developed in this study presents a distinct approach compared to the model proposed by Negi [7]. The primary difference lies in how the vaccination and infection compartments are represented, alongside the quarantine strategy employed. Our model breaks down the vaccination compartments into three doses, capturing the complexities of the vaccination program that includes both primary and booster doses. We placed an emphasis on quarantining individuals exhibiting mild symptoms, whereas those with moderate to severe symptoms were assigned to the infected compartment, highlighting differences in clinical management. Additionally, the bifurcation analysis we conducted offers insights into qualitative changes in epidemic dynamics as parameters shift, along with their biological implications.

Furthermore, we conducted model fitting on the daily COVID-19 case data in Indonesia. The results indicate that the model effectively represents disease spread trends, although it necessitates data partitioning to account for varying dynamics during specific periods. This demonstrates that our model can effectively capture the complexities of epidemiological data with the appropriate adjustments.

The Negi model [7], in contrast, consolidates the vaccination compartment into a single category while expanding the infection compartment to distinguish between symptomatic, asymptomatic, and hospitalized cases. This methodology facilitates a more profound understanding of transmission dynamics and the associated healthcare burden. Furthermore, Negi calibrated the model using disease distribution data from various countries, showcasing its capacity to effectively represent empirical data on a broad scale. Together, both models enhance our comprehension of COVID-19 dynamics. Our model focuses on the intricacies of vaccination, the quarantine of mild cases, and the representation of local data from Indonesia, whereas Negi's model offers greater detail regarding infection compartments and validation through cross-country data.

4. Conclusions

The numerical simulations indicate that the dynamics of COVID-19 spread are significantly influenced by the lambda parameter. Changes in lambda result in shifts from forward to backward bifurcation, suggesting that higher values can worsen disease spread and hinder mitigation efforts. However, some simulations show the potential for convergence towards a single point, implying the achievement of herd immunity. Thus, while an increase in lambda can complicate the situation, effective interventions may still lead to herd immunity. The simulated model adapted data on COVID-19 transmission in Indonesia. Results revealed the achievement of herd immunity in the system. The behavior of the system showed that the increase in the number of COVID-19 cases had started to converge to one value, and disease transmission was extremely minimal. This was similar to current conditions, showing that the number of COVID-19 cases no longer exists.

Author contributions: Conceptualization, MH; methodology, MH and FRF; software, FRF; validation, MH and FRF; formal analysis, MH and FRF; investigation, MH and FRF; resources, FRF; data curation, FRF; writing—original draft preparation, MH and FRF; writing—review and editing, MH and FRF; visualization, FRF; supervision, MH; project administration, FRF; funding acquisition, MH. All authors have read and agreed to the published version of the manuscript.

Conflict of interest: The authors declare no conflict of interest.

References

1. Brauer F, Castillo-Chavez C, Feng Z. Mathematical Models in Epidemiology. Springer; 2019.
2. Cooper I, Mondal A, Antonopoulos CG. A SIR model assumption for the spread of COVID-19 in different communities. Chaos, Solitons & Fractals. 2020; 139: 110057. doi: 10.1016/j.chaos.2020.110057
3. Khalaf SL, Flayyih HS. Analysis, predicting, and controlling the COVID-19 pandemic in Iraq through SIR model. Results in Control and Optimization. 2023; 10: 100214. doi: 10.1016/j.rico.2023.100214
4. Neves AGM, Guerrero G. Predicting the evolution of the COVID-19 epidemic with the A-SIR model: Lombardy, Italy and São Paulo state, Brazil. Physica D: Nonlinear Phenomena. 2020; 413: 132693. doi: 10.1016/j.physd.2020.132693
5. Zou Y, Yang W, Lai J, et al. Vaccination and Quarantine Effect on COVID-19 Transmission Dynamics Incorporating Chinese-Spring-Festival Travel Rush: Modeling and Simulations. Bulletin of Mathematical Biology. 2022; 84(2). doi: 10.1007/s11538-021-00958-5
6. Auger P, Moussaoui A. On the Threshold of Release of Confinement in an Epidemic SEIR Model Taking into Account the Protective Effect of Mask. Bulletin of Mathematical Biology. 2021; 83(4). doi: 10.1007/s11538-021-00858-8
7. Negi SS, Rana PS, Sharma N, Khatri MS. A novel SEIAHR compartment model for accessing the impact of vaccination, intervention policies, and quarantine on the COVID-19 pandemic: A case study of most affected countries Brazil, India, Italy, and USA. Computational and Applied Mathematics. 2022; 41(7). doi: 10.1007/s40314-022-01993-1
8. Yang B, Yu Z, Cai Y. The impact of vaccination on the spread of COVID-19: Studying by a mathematical model. Physica A: Statistical Mechanics and its Applications. 2022; 590: 126717. doi: 10.1016/j.physa.2021.126717
9. Tyagi S, Martha SC, Abbas S, Debbouche A. Mathematical modeling and analysis for controlling the spread of infectious diseases. Chaos, Solitons & Fractals. 2021; 144: 110707. doi: 10.1016/j.chaos.2021.110707
10. Mohammadi H, Rezapour S, Jajarmi A. On the fractional SIRD mathematical model and control for the transmission of COVID-19: The first and the second waves of the disease in Iran and Japan. ISA Transactions. 2022; 124: 103–114. doi: 10.1016/j.isatra.2021.04.012
11. Caetano C, Morgado ML, Patrício P, et al. Measuring the impact of COVID-19 vaccination and immunity waning: A modelling study for Portugal. Vaccine. 2022; 40(49): 7115–7121. doi: 10.1016/j.vaccine.2022.10.007
12. Law KB, Peariasamy KM, Mohd Ibrahim H, Abdullah NH. Modelling infectious diseases with herd immunity in a randomly mixed population. Scientific Reports. 2021; 11(1). doi: 10.1038/s41598-021-00013-2
13. MacIntyre CR, Costantino V, Trent M. Modelling of COVID-19 vaccination strategies and herd immunity, in scenarios of limited and full vaccine supply in NSW, Australia. Vaccine. 2022; 40(17): 2506–2513. doi: 10.1016/j.vaccine.2021.04.042
14. Yuan R, Jiang W, Wang Y. Saddle-node-Hopf bifurcation in a modified Leslie–Gower predator-prey model with time-delay and prey harvesting. Journal of Mathematical Analysis and Applications. 2015; 422(2): 1072–1090. doi: 10.1016/j.jmaa.2014.09.037
15. Lynch S. Dynamical Systems with Applications using Python. Springer International Publishing; 2018.
16. Castillo-Chavez C, Song B. Dynamical Models of Tuberculosis and Their Applications. Mathematical Biosciences and Engineering. 2004; 1(2): 361–404. doi: 10.3934/mbe.2004.1.361
17. Wangari IM, Stone L. Backward bifurcation and hysteresis in models of recurrent tuberculosis. PLoS One. 2018; 13(3): e0194256. doi: 10.1371/journal.pone.0194256
18. Asamoah JKK, Nyabadza F, Jin Z, et al. Backward bifurcation and sensitivity analysis for bacterial meningitis transmission dynamics with a nonlinear recovery rate. Chaos, Solitons & Fractals. 2020; 140: 110237. doi: 10.1016/j.chaos.2020.110237

19. Nadim SS, Chattopadhyay J. Occurrence of backward bifurcation and prediction of disease transmission with imperfect lockdown: A case study on COVID-19. Chaos, Solitons & Fractals. 2020; 140: 110163. doi: 10.1016/j.chaos.2020.110163
20. Omame A, Abbas M, Onyenegecha CP. Backward bifurcation and optimal control in a co-infection model for SARS-CoV-2 and ZIKV. Results in Physics. 2022; 37: 105481. doi: 10.1016/j.rinp.2022.105481
21. Nudee K, Chinviriyasit S, Chinviriyasit W. The effect of backward bifurcation in controlling measles transmission by vaccination. Chaos, Solitons & Fractals. 2019; 123: 400–412. doi: 10.1016/j.chaos.2019.04.026
22. World Health Organization. Coronavirus disease (COVID-19) pandemic. Available online: https://covid19.who.int/region/searo/country/id (accessed on 5 February 2024).
23. Toharudin T, Pontoh RS, Caraka RE, et al. National Vaccination and Local Intervention Impacts on COVID-19 Cases. Sustainability. 2021; 13(15): 8282. doi: 10.3390/su13158282
24. Djalante R, Lassa J, Setiamarga D, et al. Review and analysis of current responses to COVID-19 in Indonesia: Period of January to March 2020. Progress in Disaster Science. 2020; 6: 100091. doi: 10.1016/j.pdisas.2020.100091
25. Fahreza FR, Hasan M, Kusbudiono K. Model and Simulation of COVID-19 Transmission with Vaccination and Quarantine Interventions in Jember. InPrime: Indonesian Journal of Pure and Applied Mathematics. 2023; 5(1): 1–21. doi: 10.15408/inprime.v5i1.27192
26. Mao Y, Wang W, Ma J, et al. Reinfection rates among patients previously infected by SARS-CoV-2: Systematic review and meta-analysis. Chinese Medical Journal. 2021; 135(2): 145–152. doi: 10.1097/cm9.0000000000001892
27. Siqueira PC, Cola JP, Comerio T, et al. Herd immunity threshold for SARS-CoV-2 and vaccination effectiveness in Brazil. Jornal Brasileiro de Pneumologia. 2022; 48(2): e20210401. doi: 10.36416/1806-3756/e20210401
28. Suryawanshi YN, Biswas DA. Biswas DA. Herd Immunity to Fight Against COVID-19: A Narrative Review. Cureus. 2023; 15(1): e33575. doi: 10.7759/cureus.33575
29. Kyurkchiev N, Kyurkchiev V, Iliev A, Rahnev A. A New Modifications of the sir/seir models with “intervention polynomial factor”. methodological aspects. International Journal of Differential Equations and Applications. 2021; 20(1): 15–30.